Journal of Biomolecular NMR, **23:** 201–209, 2002.
KLUWER/ESCOM

Intraresidual HNCA: An experiment for correlating only intraresidual backbone resonances

Perttu Permi
NMR Laboratory, Structural Biology and Biophysics, Institute of Biotechnology, P.O. Box 65, FIN-00014, University of Helsinki, Helsinki, Finland (E-mail: Perttu.Permi@helsinki.fi)

Received 27 March 2002; Accepted 19 June 2002

Key words: assignment, coherence transfer, HNCA, HN(CO)CA, intraresidual HNCA, proteins, TROSY, ubiquitin

Abstract

Resonance overlap in $^{13}C^{\alpha}$-dimension can seriously deteriorate sequential assignment of proteins, especially in the case of highly alpha helical or partially unfolded structures. In this paper, two novel triple-resonance experiments, for obtaining solely intraresidual H^N, N, C^{α} correlations, are introduced. The proposed experiments are complementary to the conventional HN(CO)CA experiment, and can be utilized for the sequential assignment of $^{15}N/^{13}C/(^2H)$-labeled proteins. Coherence transfer efficiency of the new experiment is comparable to the conventional HNCA experiment on proteins with sufficiently long ^{15}N transverse relaxation time. These new coherence transfer schemes are also very useful building blocks for experiments gathering structural information, such as *J*-couplings, exclusively on the intraresidual alpha carbon. Experimental assessment is demonstrated on ubiquitin at 600 ^1H MHz.

Introduction

Isotopic enrichment of ^{15}N and ^{13}C nuclei has enabled more convenient and reliable chemical shift assignment of proteins (Bax and Grzesiek, 1993) in comparison with the conventional homonuclear NOESY/TOCSY approach (Wüthrich, 1986). The enrichment makes the so-called triple-resonance experiments viable, allowing sequential assignment by utilizing heteronuclear one- and two-bond scalar couplings for establishing sequential connectivities (Bax and Grzesiek, 1993). Consequently, several methods for obtaining sequential assignment on $^{15}N/^{13}C/(^2H)$ labeled proteins have been devised during last decade (Bax and Ikura, 1991; Kay et al., 1990; Panchal et al., 2001; Permi and Annila, 2001a,b; Sattler et al., 1999; Yamazaki et al., 1997; Yang and Kay 1999a). The most commonly employed pulse sequences for this purpose are HNCA and HN(CO)CA, or CBCANH/HNCACB and CBCA(CO)NH/HN(CO)CACB pulse schemes (Grzesiek and Bax, 1992a,b; Shan et al., 1996; Wittekind and Mueller, 1992; Yamazaki et al., 1994). These experiments correlate $^{13}C^{\alpha}$ (and $^{13}C^{\beta}$) nuclei with amide nitrogen and amide proton chemical shifts. The well-known HNCA and CBCANH/HNCACB experiments correlate *both* the intraresidual and sequential $^{13}C^{\alpha}$ (and $^{13}C^{\beta}$) chemical shifts with the intraresidual amide shifts. This alone establishes sequential assignment provided that (i) there is no substantial overlap in the spectrum and (ii) the intraresidual connectivities can be distinguished from the sequential connectivities.

Evidently, spectral overlap increases as protein size gets larger, and it is especially severe with highly alpha helical, or partially unfolded, proteins. In addition, due to comparable sizes of one- and two-bond couplings between the ^{15}N and $^{13}C^{\alpha}$ spins, it is not always easy to make a distinction between the intra- and interresidual connectivities based solely on cross peak intensities (Delaglio et al., 1991; Permi and Annila, 2001b). These quandaries will be unraveled by recording the HN(CO)CA experiment (Grzesiek and Bax, 1992a), showing exclusively sequential cross peaks, enabling unambiguous assignment of sequential connectivities while number of correlations also reduces by up to

50%, i.e., unnecessary spectral crowding decreases simultaneously. Another salient feature of this experiment is excellent coherence transfer efficiency that is clearly higher for the sequential correlation than in the corresponding HNCA experiment. However, in very large proteins at the highest magnetic fields available, the coherence transfer efficiency of the HN(CO)CA drops dramatically due to the large chemical shielding anisotropy of carbonyl carbon (Loria et al., 1999; Permi and Annila, 2001).

In this paper, we describe two intraresidual HNCA (iHNCA) pulse schemes, which are complementary experiments for HN(CO)CA, providing only *intraresidual*, i.e., $^{1}H^{N}(i)$, $^{15}N(i)$, $^{13}C^{\alpha}(i)$ connectivities. On smaller proteins at lower magnetic field strengths, the coherence transfer efficiencies are in reasonable comparison with the intraresidual correlations available in the HNCA experiment. The theoretical coherence transfer efficiency in the case of very slowly tumbling proteins at the highest magnetic fields is also estimated. These experiments can also be used as building blocks for designing sophisticated experiments to probe structural parameters, for instance measuring J-couplings or $^{13}C^{\beta}$ chemical shifts, solely on intraresidual nuclei without interference of overlapping sequential connectivities.

Material and methods

The proposed pulse schemes were exposed for experimental verification and comparison with the conventional HNCA (Bax and Ikura, 1991) and HN(CO)CA experiments (Grzesiek and Bax, 1992a) on 0.58 mM uniformly ^{15}N, ^{13}C labeled human ubiquitin (Asla Ltd., Riga, Latvia) having a molecular mass of 8.6 kDa (76 amino acid residues), dissolved in 95/5% H_2O/D_2O, 10 mM potassium phosphate buffer, pH 7.2, in a 300 µl Shigemi microcell at 30 °C. All experiments were carried out on a Varian Unity INOVA 600 NMR spectrometer, equipped with a $^{15}N/^{13}C/^{1}H$ triple-resonance probehead and an actively shielded z-axis gradient system. All spectra were acquired as two-dimensional experiments ($t_2 = 0$) using 24 transients per FID with 64, 2048 complex points and the corresponding acquisition times of 14.5 ms and 128 ms in t_1 and t_3, respectively. Delays used were $T_a = 25$ ms, $T_N = 16.6$ ms, $T_C = 4.55$ ms, $\Delta = 5.3$ ms, δ = gradient + field recovery delay. The F_1-dimension was extended by forward linear prediction to 128 complex points. The data were zero-filled to 1024 × 4096 points before Fourier transform and phase-shifted squared sine-bell window functions were applied in both dimensions.

Results and discussion

Description of the pulse sequences

The pulse sequence of the intraresidual HNCA experiment is shown in Figure 1a. The experiment mostly resembles the familiar HN(CO)CA experiment (Grzesiek and Bax, 1992a). The flow of magnetization in this novel experiment can be described as follows:

$$^{1}H^{N}\text{–}\{^{1}J_{H^{N}N}\}\text{–}^{15}N\text{–}\{^{1}J_{NC'}, ^{1}J_{NC\alpha}, ^{2}J_{NC\alpha}\}\text{–}$$
$$^{13}C'\text{–}\{^{1}J_{C'C\alpha}\}\text{–}^{13}C^{\alpha}(t_1)\text{–}^{13}C'\text{–}\{^{1}J_{C'C\alpha}\}\text{–}\{^{1}J_{NC'}$$
$$^{1}J_{NC\alpha}, ^{2}J_{NC\alpha}\}\text{–}^{15}N(t_2)\text{–}\{^{1}J_{H^{N}N}\}\text{–}^{1}H^{N}(t_3),$$

where t_i (i = 1–3) is an acquisition time for the corresponding spin and the couplings used for coherence transfer are shown in parenthesis. Initially, the longitudinal amide proton magnetization is transferred to directly bound nitrogen by the usual INEPT-fashion. During the ensuing delay $2T_a$, the one- and two-bond couplings evolve between $^{15}N(i)$ and $^{13}C^{\alpha}(i)$, $^{15}N(i)$ and $^{13}C^{\alpha}(i-1)$ spins, respectively. Additionally, one-bond coupling between $^{15}N(i)$ and $^{13}C'(i-1)$ spins evolves during the concatenated delay $2T_N$. Thus, the density operator at time point a can be described with the corresponding product operators:

$$\begin{aligned}
\sigma_a \;=\; & 2N_y(i)C'_z(i-1)\,\cos(2\pi^{1}J_{NC\alpha}T_a) \\
& \cos(2\pi^{2}J_{NC\alpha}T_a)\,\sin(2\pi J_{NC'}T_N), \\
& 2N_y(i)C^{\alpha}_z(i-1)\,\cos(2\pi^{1}J_{NC\alpha}T_a) \\
& \sin(2\pi^{2}J_{NC\alpha}T_a)\,\cos(2\pi J_{NC'}T_N), \\
& 2N_y(i)C^{\alpha}_z(i)\,\sin(2\pi^{1}J_{NC\alpha}T_a) \\
& \cos(2\pi^{2}J_{NC\alpha}T_a)\,\cos(2\pi J_{NC'}T_N), \\
& 8N_y(i)C'_z(i-1)C^{\alpha}_z(i-1)C^{\alpha}_z(i) \\
& \sin(2\pi^{1}J_{NC\alpha}T_a)\,\sin(2\pi^{2}J_{NC\alpha}T_a) \\
& \sin(2\pi J_{NC'}T_N).
\end{aligned}$$

It is worth pointing out that the delay $2T_a$ is set to ~50 ms in order to maximize the product $\sin(2\pi^{1}J_{NC\alpha}T_a)\sin(2\pi^{2}J_{NC\alpha}T_a)$. Subsequently, the magnetization is converted into the $^{13}C'$ single-quantum coherence by the succeeding 90° pulses on ^{15}N and $^{13}C'$. The two-step phase cycling on $^{13}C'$ ensures selection of only the first and the fourth term

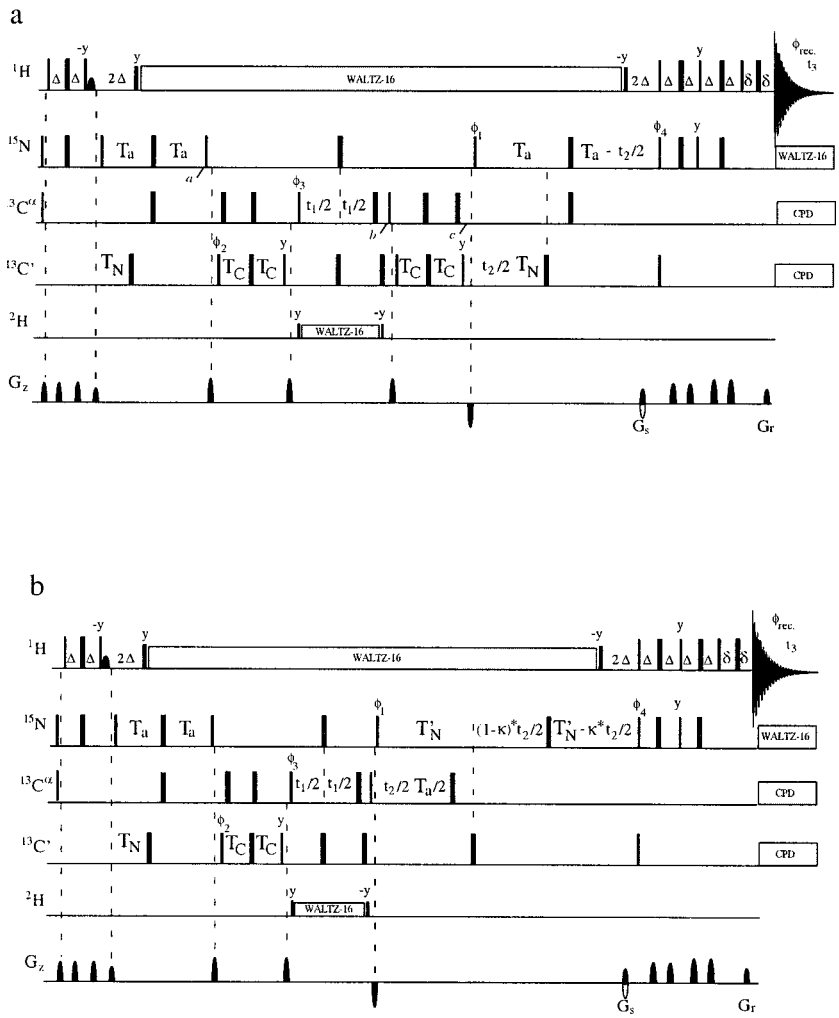

Figure 1. The intraresidual HNCA (iHNCA) experiments for recording only intraresidual correlations in $^{13}C/^{15}N/(^{2}H)$ labeled proteins. Narrow and wide bars correspond to 90° and 180° flip angles, respectively, applied with phase x unless otherwise stated. Half-ellipse denotes water selective 90° pulse to obtain water-flip-back (Grzesiek and Bax, 1993b). All 90° (180°) pulses for ^{13}C' and $^{13}C^{\alpha}$ are applied with a strength of $\Omega/\sqrt{15}$ ($\Omega/\sqrt{3}$), where Ω is the frequency difference between the centers of the $^{13}C'$ and $^{13}C^{\alpha}$ regions. The ^{1}H, ^{15}N, $^{13}C'$, and $^{13}C^{\alpha}$ carrier positions are 4.7 (water), 120 (center of ^{15}N spectral region), 175 ppm (center of $^{13}C'$ spectral region) and 56 ppm (center of $^{13}C^{\alpha}$ spectral region), respectively. The ^{13}C carrier is set initially to the $^{13}C'$ region and shifted to 56 ppm just before the 90° ϕ_3 pulse and shifted back to 175 ppm after the 90° ($^{13}C^{\alpha}$) pulse following the t_1 period. All $^{13}C'$ and $^{13}C^{\alpha}$ off-resonance pulses were applied with phase modulation by Ω. Optional deuterium decoupling can be applied during t_1 period in perdeuterated samples. Frequency discrimination in F_2 is obtained using the sensitivity-enhanced gradient selection (Kay et al., 1992; Schleucher et al., 1993). The echo and anti-echo signals are collected separately by inverting the sign of the G_s gradient pulse together with the inversion of ϕ_4. In addition to echo/anti-echo selection, ϕ_1 and ϕ_{rec} are incremented according to States-TPPI protocol (Marion et al., 1989). Quadrature detection in the $^{13}C^{\alpha}$ dimension is obtained by States-TPPI applied to ϕ_3. Pulsed field gradients were inserted as indicated for coherence transfer pathway selection and residual water suppression. The nominal delay durations are: $\Delta = 1/(4J_{HN})$; $T_N = 1/(4J_{NC'})$; $1/(4J_{NC'}) \geq T'_N \geq T_a/2$; $T_a \sim 25$ ms; $T_C = 1/(4J_{C'C^{\alpha}})$; δ = gradient + field recovery delay; $0 \leq \kappa \leq T_N/t_{2,max}$. Gradient strengths (durations): $G_s = 30$ G cm^{-1} (1.25 ms), $G_r = 29.6$ G cm^{-1} (0.125 ms). The WALTZ-16 sequence (Shaka et al., 1983) was used to decouple ^{1}H during heteronuclear coherence transfer and ^{15}N during acquisition. The GARP field was used to decouple ^{13}C during acquisition (Shaka et al., 1985). Phase cycling: ϕ_1 = x (scheme a); ϕ_1 = y (scheme b); ϕ_2 = x, −x; ϕ_3 = 2(x), 2(−x); ϕ_4 = x; $\phi_{rec.}$ = x, 2(−x), x. The last 90° ($^{13}C'$) pulse removes the dispersive contribution from the lineshape (Permi et al., 1999; Yang and Kay, 1999b).

given above. The following $^{13}C'$-$^{13}C^{\alpha}$ INEPT step converts the remaining two terms into the $^{13}C^{\alpha}$ single-quantum coherence, described by the following density operator prior to t_1 (omitting the sine terms, which are close to 1)

$$\begin{aligned}\sigma_{t1} \;=\; & 4N_z(i)C'_z(i\text{-}1)\{C^{\alpha}_y(i-1)\,\cos(2\pi^1 J_{NC}\alpha T_a)\\ & \cos(2\pi^2 J_{NC}\alpha T_a)\\ & + C^{\alpha}_y(i)\sin(2\pi^1 J_{NC}\alpha T_a)\sin(2\pi^2 J_{NC}\alpha T_a)\}.\end{aligned}$$

We should pay attention to the latter term, where the doubly antiphase $^{13}C'(i-1)$ coherence, with respect to $^{13}C^{\alpha}$, converts to the $^{13}C^{\alpha}(i)$ coherence. The $^{13}C^{\alpha}$ chemical shift is recorded during the t_1 evolution period as in the standard HN(CO)CA experiment, i.e., the magnetization can be described by the density operator (time point *b*)

$$\begin{aligned}\sigma_b \;=\; & 4N_z(i)C'_z(i-1)\{C^{\alpha}_y(i-1)\cos(2\pi^1 J_{NC}\alpha T_a)\\ & \cos(2\pi^2 J_{NC}\alpha T_a)\,\cos(\omega_C\alpha_{(i-1)}t_1)\\ & + C^{\alpha}_y(i)\,\sin(2\pi^1 J_{NC}\alpha T_a)\sin(2\pi^2 J_{NC}\alpha T_a)\\ & \cos(\omega_C\alpha_{(i)}t_1)\}\,\cos(\pi J_{C\alpha C\beta}t_1).\end{aligned}$$

After labeling the $^{13}C^{\alpha}$ chemical shift, the magnetization floats back to the amide proton by the same, but reverse coherence transfer pathway. However, the ^{15}N chemical shift is recorded during the t_2 evolution period, which is implemented into the ^{13}C-^{15}N back-INEPT in the usual constant-time manner. Hence, after Fourier transform, correlations appear at $\omega_C\alpha(i-1)$, $\omega_N(i)$, $\omega_{H^N}(i)$ and $\omega_C\alpha(i)$, $\omega_N(i)$, $\omega_{H^N}(i)$, respectively. We want to stress out that the cross peak appearing at $\omega_C\alpha(i-1)$, $\omega_N(i)$, $\omega_{H^N}(i)$, modulated by $\cos^2(2\pi^1 J_{NC}\alpha T_a)\ \cos^2(2\pi^2 J_{NC}\alpha T_a)$, arises from the undesired pathway, because it is the very same, that is, sequential correlation emerging in the HN(CO)CA spectrum. On the other hand, the cross peak appearing at $\omega_C\alpha(i)$, $\omega_N(i)$, $\omega_{H^N}(i)$, modulated by $\sin(2\pi^1 J_{NC}\alpha T_a)\ \sin(2\pi^2 J_{NC}\alpha T_a)$, corresponds to the desired *intraresidual* correlation. In practice, however, the sequential correlation does not show up in the spectrum, because it is much weaker than the *intraresidual* correlation, thanks to the $\cos^2(2\pi^1 J_{NC}\alpha T_a)\ \cos^2(2\pi^2 J_{NC}\alpha T_a)$ (≈ 0) dependence on the signal intensity (*vide infra*).

Let us now focus on the coherence transfer efficiencies in the new experiment. Transfer functions for the iHNCA and HNCA experiments are

$$\begin{aligned}&\sin^2(2\pi^1 J_{NC'}T_N)\,\sin^2(2\pi^1 J_{NC}\alpha T_a)\\ &\sin^2(2\pi^2 J_{NC}\alpha T_a)\,\sin^2(2\pi^1 J_{C'C}\alpha T_C)\\ &\exp(-4T_a/T_{2N})\,\exp(-4T_C/T_{2C'})\end{aligned} \tag{1}$$

and

$$\begin{aligned}&\sin^2(\pi^1 J_{NC}\alpha T_a)\ \cos^2(\pi^2 J_{NC}\alpha T_a)\\ &\exp(-2T_a/T_{2N}),\end{aligned} \tag{2}$$

respectively.

The nominal values for the coupling constants and delays in Equation (1) and Equation (2) are, $^1J_{NC}\alpha = 10$ Hz, $^2J_{NC}\alpha = 7$ Hz, $^1J_{NC'} = 15$ Hz, $^1J_{C'C}\alpha = 53$ Hz, $2T_a \sim 50$ ms, $2T_N \sim 33$ ms, $2T_C \sim 9.1$ ms. In the following, we assume that the transverse relaxation rates for the ^{15}N and $^{13}C'$ spins in smaller proteins are 90 and 70 ms, respectively. The corresponding coherence transfer efficiencies for the *intraresidual correlation*, for *the first* t_1 *increment* ($t_1 = 0$), in the intraresidual HNCA and conventional HNCA experiments are 0.231 and 0.207, when $^1J_{NC}\alpha$ and $^2J_{NC}\alpha$ are 10.9 Hz and 8.3 Hz, i.e., typical values found in extended structures, respectively (Figure 2). On the other hand, in alpha helical substructures, where the $^1J_{NC}\alpha$ and $^2J_{NC}\alpha$ values are predominantly close to 9.6 Hz and 6.4 Hz (Delaglio et al., 1991), respectively, the corresponding transfer throughputs are 0.18 and 0.207. In the unfolded regions, with nominal random coil values ($^1J_{NC}\alpha = 10.5$, $^2J_{NC}\alpha = 7.9$ Hz), the transfer efficiencies for the two experiments are 0.214 and 0.217, respectively. It can be realized that the coherence transfer efficiency will be higher in the iHNCA experiment provided that the ^{15}N transverse relaxation time is sufficiently long and the residues reside on beta sheet substructure or two couplings do not differ significantly from each other. On larger proteins, where the ^{15}N transverse relaxation will be faster, significant sensitivity losses will be likely because the ^{15}N coherence resides in transverse plane effectively two times longer compared to HNCA. This can be compensated for some degree with the TROSY approach (Pervushin et al., 1997), which can be implemented into the pulse sequence straightforwardly (*vide infra*). On the other hand, optimal dephasing delay for the HNCA experiment will also be closer to 15–20 ms when the relaxation is extremely fast.

Let us now consider coherence transfer efficiency for the undesired pathway, resulting in sequential correlation discussed above. We presumed that intensity

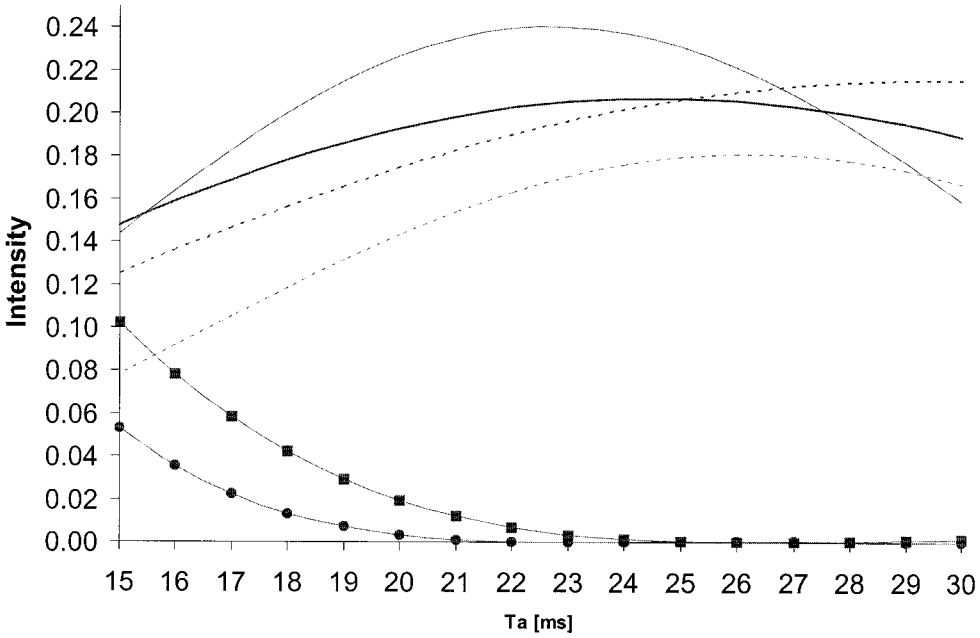

Figure 2. Coherence transfer efficiencies, for the first increment, as a function of delay T_a for the iHNCA illustrated in the Figure 1a (thin line) and the conventional HNCA (thick line) experiments. The transfer functions were calculated according to Equations 1–3, using the following parameters: $T_{2N} = 90$ ms, $T_{2C'} = 70$ ms, $2T_N = 33$ ms, $2T_C = 9$ ms, $^1J_{NC}\alpha = 10.9$ Hz and $^2J_{NC}\alpha = 8.3$ Hz (——), $^1J_{NC}\alpha = 9.6$ Hz and $^2J_{NC}\alpha = 6.4$ Hz (- - - -), $^1J_{NC'} = 15$ Hz, $^1J_{C'C}\alpha = 53$ Hz. The corresponding plots of transfer efficiencies as a function of T_a for the *undesired sequential* pathway are shown for $^1J_{NC}\alpha = 10.9$ and $^2J_{NC}\alpha = 8.3$ Hz (—●—), and for $^1J_{NC}\alpha = 9.6$ and $^2J_{NC}\alpha = 6.4$ Hz (—■—).

of the sequential cross peaks would be greatly diminished with respect to the desired intraresidual connectivities. The transfer efficiency for the sequential correlation can be given:

$$\begin{aligned}&\sin^2(2\pi^1 J_{NC'}T_N)\ \cos^2(2\pi^1 J_{NC}\alpha T_a)\\ &\cos^2(2\pi^2 J_{NC}\alpha T_a)\ \sin^2(2\pi^1 J_{C'C}\alpha T_C)\\ &\exp(-4T_a/T_{2N})\ \exp(-4T_C/T_{2C'}).\end{aligned} \tag{3}$$

In great majority of the residues, the intensity of the sequential correlation will be even two orders of magnitude lower than intraresidual correlation (Figure 2). However, in the *worst* case, the intensity of the sequential correlation can be ~25% of the intraresidual cross peak ($^1J_{NC}\alpha = 7$, $^2J_{NC}\alpha = 5$ Hz). In practice, this is rather unusual since normally $^1J_{NC}\alpha$ falls in the range of 9–12 Hz, whereas $^2J_{NC}\alpha$ samples between 6–9 Hz (Delaglio et al., 1991). In these ranges, the sequential connectivities are at least 20 times smaller than the intraresidual correlations. This can, indeed, be observed in the case of ubiquitin, where no sequential connectivities were observed although the signal to noise ratio was relatively high. It is noteworthy that the undesired term could be removed completely by the multiple-quantum filtering (Piantini et al., 1982) or by the prescription introduced by Bodenhausen and coworkers (Chiarparin et al., 2000). The relevant product operators at time point *c* are

$$\begin{aligned}\sigma_c \ =\ & 2N_z(i)C'_z(i-1) + 8N_z(i)C'_z(i-1)\\ & C^\alpha_z(i-1)C^\alpha_z(i).\end{aligned}$$

The first operator can be rejected completely by recording two data sets with and without an additional 90°($^{13}C^\alpha$) pulse applied at time point *c* while inverting receiver phase between the data sets. The caveat is a loss of sensitivity for the latter at least by the factor of $\sqrt{2}$.

Figure 3 shows expansions of two-dimensional $^{13}C^\alpha$, $^1H^N$ correlation spectra ($t_2 = 0$) recorded from ubiquitin (Asla Ltd., Riga, Latvia). The spectrum A, containing only sequential correlations, was recorded using the conventional HN(CO)CA experiment, while the spectrum B is the well-known HNCA spectrum exhibiting both the inter- and intraresidual cross peaks. The rightmost spectrum C, showing only the intraresidual $^1H^N$, ^{15}N, $^{13}C^\alpha$ connectivities, was recorded using the novel pulse sequence shown in the Figure 1a. All three spectra were recorded using the same experimental time, and with optimized

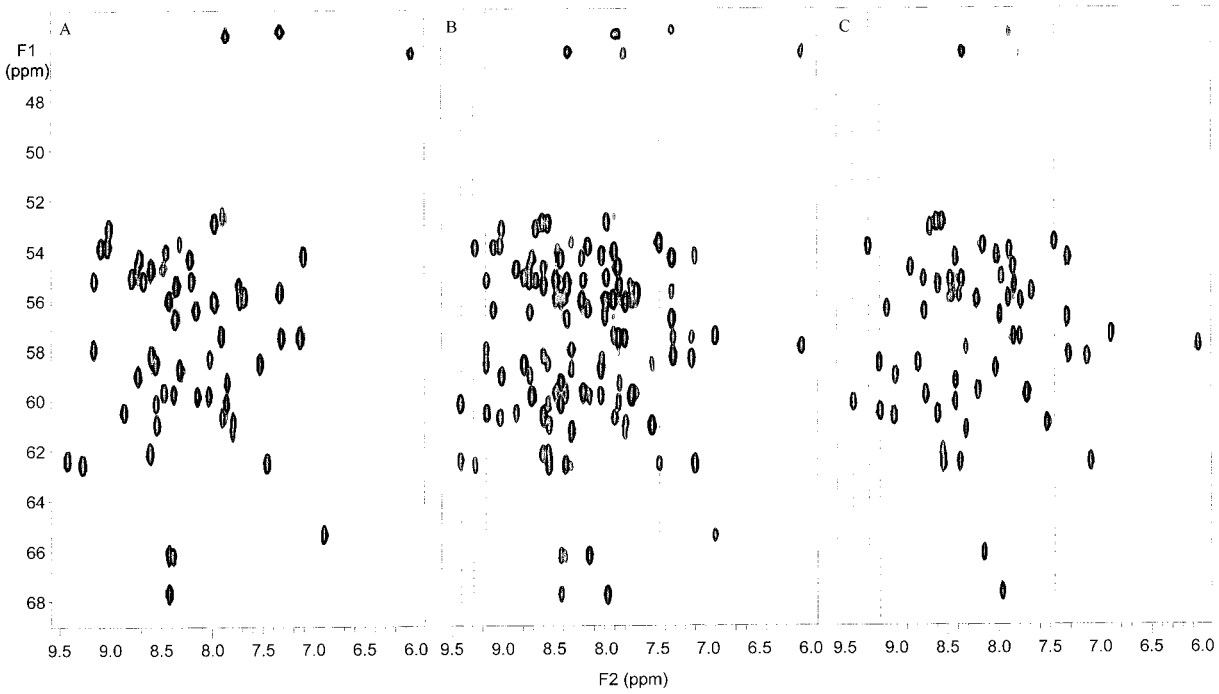

Figure 3. Expansions from the $^{13}C^{\alpha}$-$^{1}H^{N}$ regions of the HN(CO)CA (A), HNCA (B) and iHNCA (C), spectra of ubiquitin on 600 ^{1}H MHz at 30 °C. Only *sequential* cross peaks are shown in spectrum A, whereas both *sequential* and *intraresidual* correlation are visible in spectrum B. Spectrum C exhibits only *intraresidual* correlations. In spectra B and C, dashed lines indicate F_1-traces along the four residues, shown in the Figure 4.

parameters by initially monitoring the signal intensity in the 1D spectrum as a function of $N \rightarrow C^{\alpha}$ (or C') de/rephasing delay. The sensitivity of the proposed experiment is comparable to HNCA, according to theoretical anticipation, excluding some residues, which have clearly lower intensity owing to the coupling topology and faster ^{15}N transverse relaxation. It is noteworthy that in certain residues the passive $^{2,3}J_{NC}$ couplings to carbons in side-chains may also decrease the sensitivity of the iHNCA experiment with respect to the HNCA, owing to the roughly two times longer $N \rightarrow C^{\alpha}$ re/dephasing delays used in iHNCA. In addition, the coherence transfer depends on larger number of different heteronuclear couplings, which may deviate from their nominal values decreasing the coherence transfer throughput further. Figure 4 shows superposition of representative cross-sections from the HNCA (dashed line) and iHNCA (solid line) spectra along the lines denoting corresponding residues in the Figures 3B and 3C. As can be seen, clear selection of only intraresidual cross peaks is obtained, since no indication of sequential cross peaks are visible in any of the $^{13}C^{\alpha}$ traces.

By utilizing the iHNCA experiment, two slightly different strategies for obtaining sequential assignment can be employed. These are schematically presented in Figure 5. Thus, either iHNCA/HN(CO)CA or iHNCA/HNCA approach can be used. In the former scheme, solely intra- and interresidual correlations are present in two spectra, whereas in the latter approach the iHNCA spectrum, showing only intraresidual correlations, is applied for distinguishing between the sequential and intraresidual connectivities exhibiting in the HNCA spectrum. This latter method especially can be very useful in the case of very large proteins.

If one elaborates on sequential assignment of very large protein at the highest magnetic fields available (>900 MHz), it can be shown that the coherence transfer efficiency of the HN(CO)CA experiment drops dramatically due to the very large chemical shielding anisotropy of carbonyl carbon (Loria et al., 1999; Permi and Annila, 2001b). The rate of the $^{13}C'$ transverse relaxation has quadratic dependence on the magnetic field strength, and consequently, the coherence transfer pathway leading to the sequential cross peak will be more inefficient than in the HNCA, MP-HNCA and HN(CO)CANH experiments (Permi and Annila,

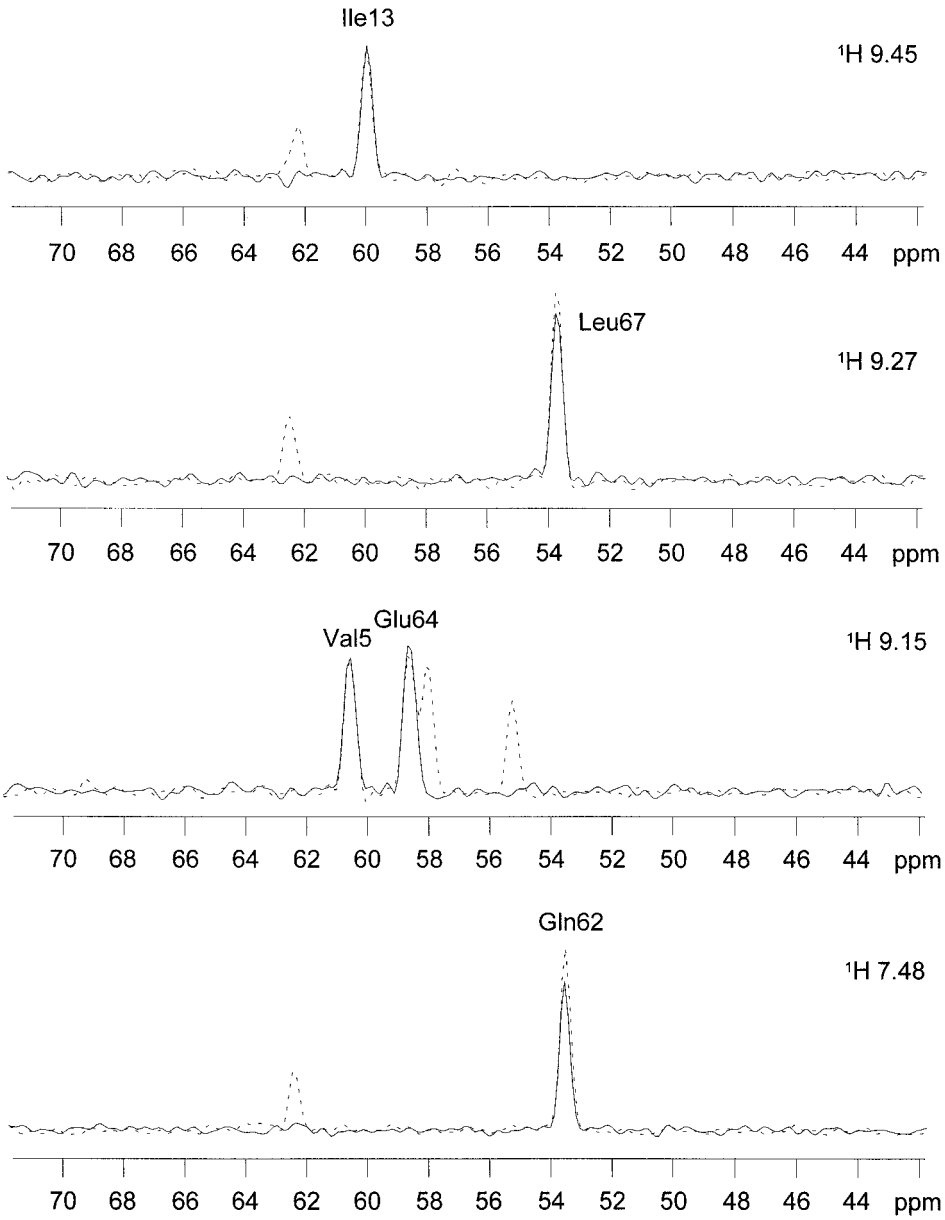

Figure 4. Four illustrating F_1-sections through the cross peaks marked with dashed lines in Figure 3.

2002). Interesting question is, whether the sequential assignment could be obtained in reverse order more efficiently, since it is not of great consequence whether solely sequential (via HN(CO)CA) or intraresidual correlations (via iHNCA) can be selected in one experiment in order to unambiguously distinguish between intra- and interresidual connectivities originating in the HNCA spectrum (see Figure 5). For this purpose, a modified version of the iHNCA experiment was devised as an alternative to HN(CO)CA at the highest field. The pulse sequence is illustrated in Figure 1b. It is basically the same experiment as iHNCA except for the ^{13}C-^{15}N back transfer following the t_1 evolution period. The pulse sequence utilizes 'out and other way back'-type coherence transfer pathway introduced earlier for the HN(CO)CANH experiment (Permi and Annila, 2002). Thus, after labeling the $^{13}C^{\alpha}$ chemical shift, the coherence is transferred directly back to the ^{15}N single quantum coherence. The back-transfer step is similar to the HNCA experiment, except that

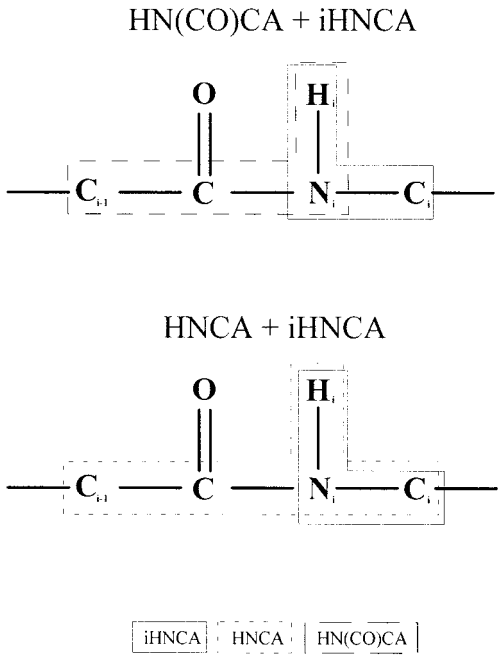

Figure 5. Two strategies for obtaining sequential assignment utilizing the iHNCA experiment. The iHNCA/HN(CO)CA strategy provides solely intra-/interresidual correlations in two spectra. In the iHNCA/HNCA approach, the iHNCA spectrum, is applied for differentiating between the sequential and intraresidual connectivities in the HNCA spectrum.

$^1J_{NC'}$ and $^1J_{NC\alpha}$ are refocused simultaneously during the concatenated delays $2T'_N$ and T_a, respectively. The desired coherence can be described as

$$2H_z^N(i)N^+(i)\ \sin(2\pi^1 J_{NC\alpha}T_a)\ \sin(2\pi^2 J_{NC\alpha}T_a)\ \sin(\pi^1 J_{NC\alpha}T_a)\ \cos(\pi^2 J_{NC\alpha}T_a)\ \cos(\omega_{C\alpha(i)}t_1)\ \cos(\pi J_{C\alpha C\beta}t_1)\ \exp(-i\omega_{N(i)}t_2), \quad (4)$$

after the ^{15}N chemical shift labeling period, which is employed in a semi-constant time manner (Grzesiek and Bax, 1993a; Logan et al., 1993) for optimal sensitivity and resolution. This leads to $\omega_{C\alpha}(i)$, $\omega_N(i)$, $\omega_{H^N}(i)$ correlation map after Fourier transform, i.e., only the intraresidual connectivities are shown. The coherence transfer efficiencies for the HN(CO)CA

$$\sin^2(2\pi J_{NC'}T_N)\ \sin^2(2\pi^1 J_{C'C\alpha}T_C)\ \exp(-4T_N/T_{2N})\ \exp(-4T_C/T_{2C'}), \quad (5)$$

and modified iHNCA

$$\sin(2\pi^1 J_{NC\alpha}T_a)\ \sin(2\pi^2 J_{NC\alpha}T_a)\ \sin(\pi^1 J_{NC\alpha}T_a)\ \cos(\pi^2 J_{NC\alpha}T_a)\ \sin(2\pi J_{NC'}T_N)\ \sin(2\pi J_{NC'}T'_N) \times \sin(2\pi^1 J_{C'C\alpha}T_C)\ \exp(-3T_a/T_{2N})\ \exp(-2T_C/T_{2C'}), \quad (6)$$

experiments can be calculated for their differing parts using the constants given above except for the transverse relaxation times, which are now assumed to be 50 and 6 ms for the ^{15}N and $^{13}C'$ spins in a very large protein at the highest field, respectively (Permi and Annila, 2002). The coherence transfer throughput in iHNCA, using the values given above, yields value of 0.038 (0.034) for $^1J_{NC\alpha} = 10.9$ (9.6) Hz, $^2J_{NC\alpha} = 8.3$ (6.4) Hz and $T_a = 12.5$ ms. The corresponding coherence transfer efficiency for the conventional HN(CO)CA experiment is 0.032 (Permi and Annila, 2002). Therefore, the sensitivity of the modified iHNCA experiment is competitive for the HN(CO)CA scheme, and consequently, it can be very useful for obtaining sequential assignment of very large proteins together with the HNCA experiment as an alternative to the familiar HNCA/HN(CO)CA approach. It should be noted that Figure 1b shows non-TROSY version of the experiment. The modifications needed for the TROSY implementation are (i) removal of the first 90° (^{15}N) pulse as well as removal of proton and nitrogen decoupling fields, and (ii) replacement of the ^{15}N-^1H back-INEPT with one of the several TROSY building blocks available (Andersson et al., 1998; Meissner et al., 1998; Pervushin et al., 1998; Rance et al., 1999; Weigelt, 1999; Yang and Kay, 1999b).

As in the case of another intraresidual HNCA pulse scheme, the undesired pathway will lead to the sequential cross peak in the modified iHNCA experiment. The coherence transfer efficiency for this undesired pathway can be given:

$$\cos(2\pi^1 J_{NC\alpha}T_a)\ \cos(2\pi^2 J_{NC\alpha}T_a)\ \cos(\pi^1 J_{NC\alpha}T_a)\ \sin(\pi^2 J_{NC\alpha}T_a)\ \sin(2\pi J_{NC'}T_N)\ \sin(2\pi J_{NC'}T'_N) \times \sin(2\pi^1 J_{C'C\alpha}T_C)\ \exp(-3T_a/T_{2N})\ \exp(-2T_C/T_{2C'}). \quad (7)$$

Again, the undesired sequential correlation will be at least 15 times smaller in intensity than the corresponding intraresidual cross peak in the surface restrained by the $^1J_{NC\alpha}$ and $^2J_{NC\alpha}$ couplings sampling between the values 9–12 and 6–9 Hz, respectively.

Conclusions

We have presented two new pulse schemes establishing solely intraresidual connectivities in ^{15}N, ^{13}C, (^2H)-labeled proteins. The experiments are complementary for the familiar HN(CO)CA experiment,

which shows only sequential connectivities. Consequently, the proposed experiments can used for the sequential assignment in an analogous manner, i.e., distinguishing intraresidual cross peaks from sequential connectivities while avoiding unnecessary spectral crowding. It is also possible to spread coherence transfer out to the *intraresidual* $^{13}C^{\beta}$ spin, similar to the HN(CO)CACB experiment. Moreover, these novel experiments can be expanded for retrieving structural information such as *J*-couplings on spectra containing exclusively intraresidual nuclei.

Acknowledgements

This work was financially supported by the Ministry of Education.

References

Asla Ltd. http://www.asla-biotech.com

Bax, A. and Grzesiek, S. (1993) *Acc. Chem. Res.*, **26**, 131–138.

Bax, A. and Ikura, M. (1991) *J. Biomol. NMR*, **1**, 99–104.

Chiarparin, E., Pelupessy, P., Ghose, R. and Bodenhausen, G. (2000) *J. Am. Chem. Soc.*, **122**, 1758–1761.

Delaglio, F., Torchia, D.A. and Bax, A. (1991) *J. Biomol. NMR*, **1**, 439–446.

Grzesiek, S. and Bax, A. (1992a) *J. Magn. Reson.* **99**, 201–207.

Grzesiek, S. and Bax, A. (1992b) *J. Am. Chem. Soc.* **114**, 6291–6293.

Grzesiek, S. and Bax, A. (1993a) *J. Biomol. NMR* **3**, 185–204.

Grzesiek, S. and Bax, A. (1993b) *J. Am. Chem. Soc.*, **115**, 12593–12594.

Kay, L.E., Ikura, M., Tschudin, R. and Bax, A. (1990) *J. Magn. Reson.*, **89**, 496–514.

Kay, L.E., Keifer, P. and Saarinen, T. (1992) *J. Am. Chem. Soc.*, **114**, 10663–10665.

Logan, T.M., Olejniczak, E.T., Xu, R.X. and Fesik, S.W. (1993) *J. Biomol. NMR*, **3**, 225–231.

Loria, J.P., Rance, M. and Palmer III, A.G. (1999) *J. Magn. Reson.*, **141**, 180–184.

Marion, D., Ikura, M., Tschudin, R. and Bax, A. (1989) *J. Magn. Reson.*, **85**, 393–399.

Meissner, A., Schulte-Herbrüggen, T., Briand, J. and Sørensen, O.W. (1998) *Mol. Phys.*, **95**, 1137–1142.

Panchal, S.C., Bhavesh, N.S. and Hosur, R.V. (2001) *J. Biomol. NMR*, **20**, 135–147.

Permi, P., Sorsa, T., Kilpeläinen, I. and Annila, A. (1999) *J. Magn. Reson.*, **141**, 44–51.

Permi, P. and Annila, A. (2001a) *Magn. Res. Chem.*, **39**, 179–181.

Permi, P. and Annila, A. (2001b) *J. Biomol. NMR*, **20**, 127–133.

Permi, P. and Annila, A. (2002) *J. Magn. Reson.*, **155**, 123–130.

Pervushin, K., Riek, R., Wider, G. and Wüthrich, K. (1997) *Proc. Natl. Acad. Sci. USA*, **94**, 12366–12371.

Pervushin, K.V., Wider, G. and Wüthrich, K. (1998) *J. Biomol. NMR*, **12**, 345–348.

Piantini, U., Sørensen, O.W. and Ernst, R. (1982) *J. Am. Chem. Soc.*, **104**, 6800–6801.

Rance, M., Loria, P. and Palmer, A.G., III. (1999) *J. Magn. Reson.*, **136**, 92–101.

Sattler, M., Schleucher, J. and Griesinger, C. (1999) *Prog. Nucl. Magn. Reson. Spectr.*, **34**, 93–158.

Schleucher, J., Sattler, M. and Griesinger, C. (1993) *Angew. Chem. Int. Ed. Engl.*, **32**, 1489–1491.

Shaka, A.J., Keeler, J., Frenkiel, T. and Freeman, R. (1983) *J. Magn. Reson.*, **52**, 335–338.

Shaka, A.J., Parker, P.B. and Freeman, R. (1985) *J. Magn. Reson.*, **64**, 547–552.

Shan, X., Gardner, K.H., Muhandiram, D.R., Rao, N.S., Arrowsmith, C.H., and Kay, L.E. (1996) *J. Am. Chem. Soc.*, **118**, 6570–6579.

Weigelt, J. (1998) *J. Am. Chem. Soc.*, **120**, 10778–10779.

Wittekind, M. and Mueller, L. (1992) *J. Magn. Reson.*, **101B**, 201–205.

Wüthrich, K. (1986) *NMR of Proteins and Nucleic Acids*, John Wiley and Sons, New York, NY.

Yamazaki, T., Lee, W., Revington, M., Mattiello, D.L., Dahlquist, F.W., Arrowsmith, C.H. and Kay, L.E. (1994) *J. Am. Chem. Soc.*, **116**, 6464–6465.

Yamazaki, T., Tochio, H., Furui, J., Aimoto, S. and Kyogoku, Y. (1997) *J. Am. Chem. Soc.*, **120**, 872–880.

Yang, D. and Kay, L.E. (1999a) *J. Am. Chem. Soc.*, **121**, 2571–2575.

Yang, D. and Kay, L.E. (1999b) *J. Biomol. NMR*, **13**, 3–9.